Absorption of Laser Light in Overdense Plasmas by Sheath Inverse Bremsstrahlung

T. Y. B. Yang

W. L. Kruer

R. M. More

A. B. Langdon

Introduction

In recent years, there has been increasing interest in the interaction of short laser pulses with overdense plasmas.[1–12] For sufficiently short laser pulses, the hydrodynamic motion of the heated target does not play a dominant role, and the production of high-density plasmas with sharp density gradients becomes feasible. One topic of great interest is the dependence of the light absorption on the laser intensity and plasma temperature in such plasmas.

In the Fast Ignitor concept[13] of inertial confinement fusion, the core is ignited with super-thermal electrons generated by the high-intensity ignition laser. It is expected that the absorption of the laser energy occurs at a steep gradient produced by the hole-drilling laser. Furthermore, the absorption is mainly due to collisionless mechanisms such as the one discussed in this article. Although the intensity of the ignition laser is expected to be so high that the assumption of the present linear analysis is no longer valid, certain aspects of the present analysis still hold true. For example, the transverse electron temperature is invariant for normal incidence case, unless surface rippling happens. Also, the comparison between the analytical and numerical results provides some criteria in determining parameters (e.g., grid size and time step) used in numerical simulations, which will be heavily relied on in the regime of the Fast Ignitor where analytical analysis may not be tractable.

It has been observed in laser absorption experiments[1–3] that, starting from a sufficiently low intensity, the absorption rate of light in overdense plasmas increases as a function of laser intensity until it reaches the "resistivity saturation,"[1] a condition in which the electron mean-free path in the plasma reaches a minimum value. Further increase of the laser intensity and the plasma temperature will then cause an increase in the electron mean-free path and a decrease in the absorption rate. When the electron mean-free path is longer than the skin depth, theoretical studies[14–16] suggest that collisionless absorption mechanisms such as the sheath inverse bremsstrahlung[14] and the anomalous skin effect[15–19] become important.

In this article, we modify the original sheath inverse bremmstrahlung model[14] by including the $\mathbf{v} \times \mathbf{B}$ (velocity and magnetic field, respectively) term in the Lorentz force equation, since the evanescent magnetic field in an overdense plasma is greater than the corresponding electric field. Our results are significantly different from those derived without the $\mathbf{v} \times \mathbf{B}$ term, except when the distribution function is isotropic $[f_0(\mathbf{v}) = f_0(|\mathbf{v}|)]$. For an isotropic distribution function, identical results will be obtained whether or not the $\mathbf{v} \times \mathbf{B}$ term in the equation of motion is included in the derivation. However, if the $\mathbf{v} \times \mathbf{B}$ term were neglected, the absorption of the light would be incorrectly interpreted as an increase in the transverse electron temperature, while the conservation of the transverse components of the canonical momentum requires that, after leaving the interaction region ($|x| \lesssim \delta$), an electron should have the same transverse momentum as it did before it entered the interaction region.

By deriving the absorption coefficients for both the sheath inverse bremsstrahlung and the anomalous skin effect from the same set of equations, we show that both phenomena are limiting cases of the same collisionless absorption mechanism. The sheath inverse bremsstrahlung corresponds to the limit where $\omega^2 c^2 >> \omega_p^2 v_e^2$, while the anomalous skin effect corresponds to $\omega^2 c^2 << \omega_p^2 v_e^2$.

We have carried out numerical simulations of the light absorption in overdense plasmas using the particle-in-cell (PIC) plasma simulation code ZOHAR.[20] The absorption coefficients observed in the simulations are in reasonable agreement with the values calculated from the linear theory. We have investigated the effects of finite density gradients with ZOHAR simulations.

Theoretical Model for the Sheath Inverse Bremsstrahlung Absorption and the Anomalous Skin Effect

The model consists of an overdense plasma filling the half-space $x > 0$, and electric and magnetic fields of the following forms, respectively:

$$E_y(x,t) = \mathrm{Re}\left\{E_0 \exp\left[i(kx \pm \omega t)\right]\right\} \quad ,$$

$$B_z(x,t) = \mathrm{Re}\left\{\frac{ck}{\omega} E_0 \exp\left[i(kx \pm \omega t)\right]\right\} \quad . \qquad (1)$$

Here, x is the propagation direction, E_0 and ω are real-valued constants, and k is the wave vector. Immobile ions, with zero density for $x < 0$ and a constant density for $x > 0$, are assumed to form the neutralizing background. The plasma is assumed to be highly overdense ($\omega_p^2 >> \omega^2$) and the fiducial thermal velocity v_e, which characterizes the electron distribution, is sufficiently small ($\omega^2 c^2 >> \omega_p^2 v_e^2$). Except in the sheath regime near $x = 0$, the electron density n_e is equal to n_0 for $x > 0$ and is zero for $x < 0$. When an electron hits the sheath ($x = 0$) from the right ($x > 0$), instantaneous specular reflection is assumed, i.e., the y and z components of the momentum remain unchanged while the x component reverses with the amplitude unchanged. Since the typical time scale to reverse electron momentum in the sheath region is $1/\omega_p$, which is much shorter than both the wave period ($2\pi/\omega$) and the transit time in the skin depth ($c/v_e\omega_p$) in an overdense nonrelativistic plasma, instantaneous reflection is a reasonable assumption. Here, $\omega_p = (4\pi n_0 e^2/m_e)^{1/2}$ is the electron plasma frequency. The assumption of specular reflection requires that the sheath be one-dimensional (1-D), i.e., that the scale length of the transverse variation be much longer than the width of the sheath (approximately equal to the Debye length). The present analysis also assumes that the quiver velocity $v_{os} = eE_0/m_e\omega$ is much smaller than the fiducial thermal velocity v_e, so that the perturbation analysis is applicable.

In a recent paper,[21] the power transferred from the laser to the plasma per unit area of laser–plasma interface was derived from the equation of motion, giving

$$P_{ab} = \frac{2n_0 e^2 E_0^2 \delta^2}{m_e} \int d^2 v_\perp \int_0^\infty dv_x \frac{v_x v_y^2 \left(\omega^2\delta^2 \pm v_x^2\right)}{\left(\omega^2\delta^2 \pm v_x^2\right)^3} f_0(\mathbf{v}) \quad , \qquad (2)$$

where $\delta = i/k$. A similar derivation without the $\mathbf{v} \times \mathbf{B}$ term in the equation of motion will give

$$P_{ab} = \frac{n_0 e^2 E_0^2 \delta^2}{m} \int d^2 v_\perp \int_0^\infty dv_x \frac{v_x^3}{\left(\omega^2\delta^2 + v_x^2\right)^2} f_0(\mathbf{v}) \quad . \qquad (3)$$

For an isotropic distribution function [$f_0(\mathbf{v}) = f_0(|\mathbf{v}|)$], Eq. (3) is equivalent to Eq. (2). For general distribution functions, however, Eq. (3) gives an absorption rate significantly different from Eq. (2).[21] Moreover, if the $\mathbf{v} \times \mathbf{B}$ term had been neglected, the absorption of the light would be incorrectly interpreted as an increase in the transverse (y-direction) electron temperature, while the conservation of the transverse components of the canonical momentum requires that, after leaving the interaction region ($|x| \lesssim \delta$), an electron should have the same y-momentum as it did before it entered the interaction region.

To show the relation between the sheath inverse bremsstrahlung and the anomalous skin effect, we follow the usual treatment of the anomalous skin effect[15–19] and extend the plasma and the electromagnetic fields in the present model to the half space $x < 0$ with

$$E_y(\pm x) = E_y(x), \quad B_z(\pm x) = \pm B_z(x) \quad . \qquad (4)$$

The discontinuity in B_z requires a current sheet $\mathbf{J} = \hat{e}_y J_0 \delta(x) \exp(-i\omega t)$, whose amplitude is determined by

$$B_z\left(x = 0^+\right) \pm B_z\left(x = 0^\pm\right) = 2B_z\left(x = 0^+\right). \qquad (5)$$

Since an electron with $x > 0$ in the extended model will have the same orbits as the corresponding electron in the original model, the two models are equivalent as far as the region $x > 0$ is concerned. In the extended model, the electric field satisfies the equation

$$\left(c^2 \frac{\partial^2}{\partial x^2} + \omega^2\right) E_y(x) = \pm 4\pi i\omega \left[j_y(x) + J_0\delta(x)\right] \quad , \qquad (6)$$

where $j_y(x)$ is the current density induced by the electromagnetic fields. Performing the Fourier transform on Eq. (6), and making use of the well known relation[22] between the induced current density j_y and the electric field E_y, it follows that

$$\hat{E}_y(k) = \frac{\pm 4\pi i\omega J_0}{D(\omega, k)} \quad , \qquad (7)$$

and

$$D(\omega, k) = \omega^2 \pm c^2 k^2 \pm \omega_p^2 \left[1 \pm \int d^3 v \frac{k v_y^2}{\omega \pm k v_x} \frac{\partial f_0}{\partial v_x}\right] \quad . \qquad (8)$$

Here, $\hat{E}_y(k)$ is the Fourier transform of $E_y(x)$.

In the regime of the anomalous skin effect ($\omega^2 c^2 << \omega_p^2 v_e^2$ and $\omega_p^2 >> \omega^2$), and for an isotropic distribution function [$f_0(\mathbf{v}) = f_0(|\mathbf{v}|)$], making the

appropriate approximation[21] of the function $D(\omega,k)$ gives the absorption coefficient

$$\eta_{as} = \frac{8\omega\delta_{as}}{3\sqrt{3}c} \quad . \tag{9}$$

It was also shown in Ref. 21 that the appropriate approximation of the function $D(\omega,k)$ in the $\omega^2c^2 >> \omega_p^2 v_e^2$ limit reproduces the power absorption of the sheath inverse bremsstrahlung given in Eq. (2). The corresponding absorption coefficient is

$$\eta_{sib} = \pm\frac{8\omega^2\omega_p^2\delta^4}{c\left(\omega^2\delta^2 + c^2\right)}\int d^2v_\perp v_y^2\int_0^\infty dv_x\,\frac{v_x^2}{\left(\omega^2\delta^2 + v_x^2\right)^2}\frac{\partial f_0}{\partial v_x}$$

$$= \frac{16\omega^2\delta^2}{c}\left[\int d^2v_\perp v_y^2\int_0^\infty dv_x\,\frac{v_x\left(\omega^2\delta^2 \pm v_x^2\right)}{\left(\omega^2\delta^2 + v_x^2\right)^3}f_0(\mathrm{v})\right]$$

$$\times\left[1 \pm \int d^3v\,\frac{v_y^2(\omega^2\delta^2 - v_x^2}{\left(\omega^2\delta^2 + v_x^2\right)^2}f_0(\mathrm{v})\right]^{\pm1} \quad . \tag{10}$$

The sheath inverse bremsstrahlung and the anomalous skin effect are two limiting cases of a more general collisionless absorption mechanism described by Eqs. (7) and (8). The sheath inverse bremsstrahlung corresponds to the limit where $\omega^2c^2 >> \omega_p^2 v_e^2$, while the anomalous skin effect corresponds to $\omega^2c^2 << \omega_p^2 v_e^2$. In the intermediate regime ($\omega^2c^2 \approx \omega_p^2 v_e^2$), the absorption coefficient can be obtained by performing the inverse Fourier transform of Eqs. (7) and (8).

For a plasma with Maxwellian distribution function

$$f_0(\mathbf{v}) = \frac{1}{\left(2\pi v_e^2\right)^{3/2}}\exp\left(\pm\frac{|\mathbf{v}|^2}{2v_e^2}\right) \quad , \tag{11}$$

Eq. (10) reduces to a closed analytic form

$$\eta_{sib} = \frac{8}{\sqrt{2\pi}}\frac{v_e}{c}\,a\left[(a+1)\exp(a)E_1(a) \pm 1\right]$$

$$\times\left[\frac{1}{2} + \frac{\sqrt{\pi a}}{2}\exp(a)\mathrm{erfc}\left(\sqrt{a}\right)\right]^{\pm1} \quad , \tag{12}$$

where

$$a = \frac{\omega^2\delta^2}{2v_e^2}, \quad E_1(a) = \int_0^\infty \frac{\exp(\pm t)}{t}\,dt \quad ,$$

and

$$\mathrm{erfc}(z) = \frac{2}{\sqrt{\pi}}\int_z^\infty \exp\left(\pm t^2\right)dt \quad . \tag{13}$$

As can be seen from Eq. (12), the quantity $\eta_{sib}c/v_e$ depends on the system parameters only through the dimensionless parameter $\omega\delta/v_e$, which is approximately the ratio of the transit time in the collisionless skin depth over the period of the incident light. This result will be compared with the more accurate result calculated from Eqs. (7) and (8), i.e.,

$$\eta_{ab} = \frac{8\sqrt{2}}{\pi}\frac{v_e}{c}\,\mathrm{Im}\left(\int_0^\infty d\xi\,\frac{1}{1 \pm \frac{\xi^3}{b^2}Z(\xi)}\right) \quad , \tag{14}$$

where $b^2 = \omega_2c_2/2\,\omega_p^2 v_e^2$ and $Z(x)$ is the plasma dispersion function.[23] Equation (14) was derived in Ref. 21.

Figure 1 plots the quantities $\eta_{ab}c/v_e$ (Exact) calculated numerically from Eq. (14), $\eta_{sib}c/v_e$ (SIB) calculated from Eq. (12), and $\eta_{as}c/v_e$ (ASE) defined in Eq. (9). The curves are plotted versus $\omega^2c^2/\omega_p^2 v_e^2$ in Fig. 1. It can be seen that both $\eta_{sib}c/v_e$ and $\eta_{as}c/v_e$ are in good agreement with $\eta_{ab}c/v_e$, in their respective regimes of validity. It is worth reiterating that, for an isotropic distribution function $[f_0(\mathbf{v}) = f_0(|\mathbf{v}|)]$, such as the one in Eq. (11), an identical absorption coefficient would be obtained whether or not the $\mathbf{v}\times\mathbf{B}$ term in the equation of motion was included in the derivation. However, neglecting the $\mathbf{v}\times\mathbf{B}$ term will lead to an incorrect interpretation of the absorption mechanism.

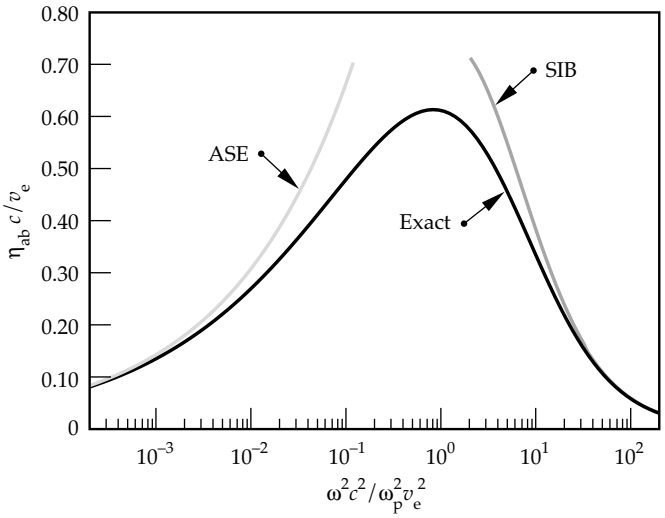

FIGURE 1. The quantities $\eta_{ab}c/v_e$ (Exact) calculated numerically from Eq. (14), $\eta_{sib}c/v_e$ (SIB) calculated from Eq. (12), and $\eta_{as}c/v_e$ (ASE) defined in Eq. (9). The curves are plotted versus $\omega^2c^2/\omega_p^2 v_e^2$. (08-00-0296-0388pb01)

Numerical Simulations of the Light Absorption in Overdense Plasmas

To examine the validity of the absorption coefficient derived in the previous section, we have carried out several runs of numerical simulations using the PIC plasma simulation code ZOHAR.[20] In all the simulations, the electric field of the incident light E_{in} satisfies $E_{in}^2 << \pi n_0 m_e v_e^2$ so that the quiver velocity of electrons in the overdense plasma is smaller than the thermal velocity, as was assumed in the analytical derivation of the absorption coefficient. The 1-D simulations are set up as follows:

1. The electromagnetic fields can vary only in the x direction. The length of the simulation region is $l_x = 40c/\omega_p$.
2. The boundary conditions of the electromagnetic fields at $x = 0$ correspond to a normally incident circularly polarized plane wave. The amplitude of the wave gradually increases from zero at the beginning of the simulation ($t = 0$) to a value E_{in} at the end of the fifth wave period. The amplitude of the incident wave remains constant thereafter.
3. The wave impedances of the boundaries are chosen such that the outgoing waves will be completely reflected at $x = l_x$ and completely transmitted at $x = 0$.
4. The initial electron density n_e is zero for $0 < x < 3l_x/4$, and is equal to a constant value n_0 for $3l_x/4 < x < l_x$. Immobile neutralizing background charge density with the same profile as that of n_e is imposed to ensure charge neutrality at $t = 0$.
5. At $t = 0$, simulation particles are loaded uniformly in the region $3l_x/4 < x < l_x$, with Maxwellian distribution in the velocity space.
6. During the simulation, particles that hit the right boundary at $x = l_x$ are re-emitted according to the Maxwellian distribution, with the same thermal velocity v_e as the initial distribution function.
7. For particles moving to the left, we have used two types of reflection conditions, as will be described later.

Three sets of simulations have been carried out, with the initial thermal velocity v_e equal to $0.1c$. Each set consists of simulations with different values of ω/ω_p. The simulation parameters are (i) 800 equally spaced grid points for the electromagnetic fields; (ii) 409,600 simulation particles; (iii) the time step $\Delta t = 0.04/\omega_p$. The total numbers of time steps N_t are $N_t = 80{,}000/\omega_p$ for the simulations with $(\omega c/\omega_p v_e)^2$ equal to 0.1 or 0.2, and $N_t = 40{,}000/\omega_p$ for the rest. There are three differences between the three sets of simulations: (1) For the first set of simulations, the particles that reach the laser–plasma interface at $x = 3l_x/4$ are reflected specularly, and the longitudinal electric field (E_x) is purposely turned off to mimic the idealized model of the linear theory. (2) For the second and the third sets of simulations, the self-consistent longitudinal electric field (E_x) remains on, and the particles that reach the left simulation boundary at $x = 0$ are specularly reflected. However, only a few particles ever reach the left boundary—most of the particles are reflected by the sheath electric field in the vicinity of $x = 3l_x/4$. (3) The steady-state value of laser intensity for the first and second sets is $(eE_{in}/\omega_p m_e c)^2 = \wp_{in} = 10^{-5}$, and that for the third set is $\wp_{in} = 2.5 \times 10^{-4}$.

Figure 2 compares the absorption coefficients observed in the simulations with those calculated numerically from Eq. (14). The absorption coefficients

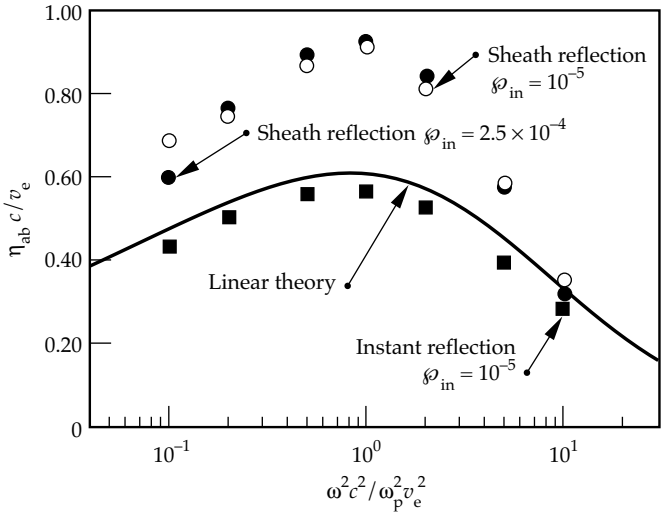

FIGURE 2. A comparison of the absorption coefficients times c/v_e observed in the PIC simulations with those from the linear theory. (08-00-0296-0389pb01)

from the first set of simulations (solid squares) agree quite well with the linear theory, while those from the second set (open circles) and the third set (solid circles) are significantly greater than predicted by the linear theory, except those with $(\omega c/\omega_p v_e)^2 = 10$. A plausible explanation of the discrepancy is that the linear theory assumes instant reflection in the sheath region, while the finite reflection time may play an important role in those simulations. This explanation is supported by the agreement between the linear theory and results from the first set of simulations, where instant specular reflection condition is imposed at the laser–plasma interface at $x = 3l_x/4$. The comparison between the second and third sets of simulations indicates that most of the simulations are in the linear regime, since the absorption coefficients are not very sensitive to the intensity of the incident laser light. The exceptional cases are those with $(\omega c/\omega_p v_e)^2 = 0.1$, for which the nonlinear effects may have set in when $\wp_{in} = 2.5 \times 10^{-4}$.

In the simulations, the flows of the electromagnetic energy and the electron kinetic energy through the boundaries at $x = 0$ and $x = l_x$ are taken into account, therefore corresponding to the net transfer of the electromagnetic energy into the electron kinetic energy as shown in Fig. 2. The total (electromagnetic plus kinetic) energy is conserved very well in the simulations, with the change in the total energy (ΔE_{total}) no more than 1% of the net increase in the electron kinetic energy (ΔE_e).

As mentioned earlier, the transverse components of the canonical momentum are the constants of the motion in the present 1-D model. This is confirmed by the distributions of the momentum observed in the simulations, which show hardly any changes in the distributions of p_y and p_z. The absorption of the electromagnetic energy, therefore, must be accompanied with the change in the distribution of the longitudinal momentum p_x.

Figure 3 compares the distributions $N(/m_e c)$ of the normalized longitudinal momentum $p_x/m_e c$ at the ends of three PIC simulations (black line) with those at the beginnings of the simulations (gray line). We obtain the distributions by sorting the simulation particles into bins of width $\Delta p_x/m_e c = 0.02$. Only particles located in the interval $7l_x/8 \le x \le l_x$ are counted, so that all the particles counted are at least $5c/\omega_p$ away from the laser–plasma interface. Figures 3(a) and 3(b) correspond to the solid squares in Fig. 2, with $(\omega c/\omega_p v_e)^2$ equal to 0.1 and 1.0, respectively. Figure 3(c) is obtained from a simulation similar to the one corresponding to the solid square with $(\omega c/\omega_p v_e)^2$ equal to 10, except that $\wp_{in} = 10^{-3}$ so that the difference between the initial and the final distributions can be seen easily. The absorption coefficient observed in the simulation for Fig. 3(c) is 0.0327, which is very close to the value 0.0324 for $\wp_{in} = 2.5 \times 10^{-4}$ shown in Fig. 2 (the solid square at $\omega^2 c^2/\omega_p^2 v_e^2 = 10$).

In Figs. 3(a) and 3(b), significant differences between the initial and the final distributions can be seen clearly for $p_x > 0$. Because the parameters ω_p and v_e are the same for all three simulations, the comparison between the three final distributions in Figs. 3(a) and 3(b) indicates that as ω becomes smaller, the change in $N(p_x/m_e c)$ shifts to smaller p_x. A possible implication of this trend is that the breakdown of the linear theory, which assumes that the unperturbed velocity is greater than the quiver velocity $v_{os} = eE_0/m_e\omega$, may set in at a smaller E_0 when ω decreases. For the case in Fig. 3(a), sizable changes in $N(p_x/m_e c)$ can be seen even for negative p_x. This can explain the considerable decrease in the absorption coefficient, for the cases with $(\omega c/\omega_p v_e)^2 = 0.1$ in Fig. 2, as $\wp_{in}$ increases from 10^{-5} (open circle) to 2.5×10^{-4} (solid circle).

The results described so far are obtained from simulations with the sharpest density gradient possible, i.e., the densities of the immobile ions increase from zero to the maximum values within one grid separation, $\Delta x = 0.05c/\omega_p$. To study the effects of finite density gradients, we have also carried out three sets of simulations consisting of runs all having a linear ramp in their ion density profile. The width of the ramp L varies over a wide range of values. The initial n_e profile in each run coincides with the ion density profile. The laser intensity corresponds to $(eE_{in}/\omega_p m_e c)^2 = \wp_{in} = 10^{-5}$, and the thermal velocity is $v_e = 0.1c$. The rest of the simulation parameters are similar to those described earlier in this section.

In Tables 1(a)–(c), absorption coefficients η obtained from these simulations are shown versus the widths L of the density ramp. Each of the three panels corresponds to a set of simulations with a fixed $(\omega_p/\omega)^2$ (100, 50, or 20). For $(\omega_p/\omega)^2 = 100$, panel (a) clearly shows that η, as a function of L, has a maximum value approximately equal to 11.5% with $L\omega_p/c$ between 2 and 3. Panel (b) shows a similar dependence of η on L for $(\omega_p/\omega)^2 = 50$, with the maximum η of 9.5% occurring around $L\omega_p/c = 1.5$. For $(\omega_p/\omega)^2 = 20$, panel (c) shows no increase in η for small $L\omega_p/c$. Although we might have caught the increasing trend in η for $(\omega_p/\omega)^2 = 20$ had we run more simulations with finer grid separations, we do not expect to see much increase in η.

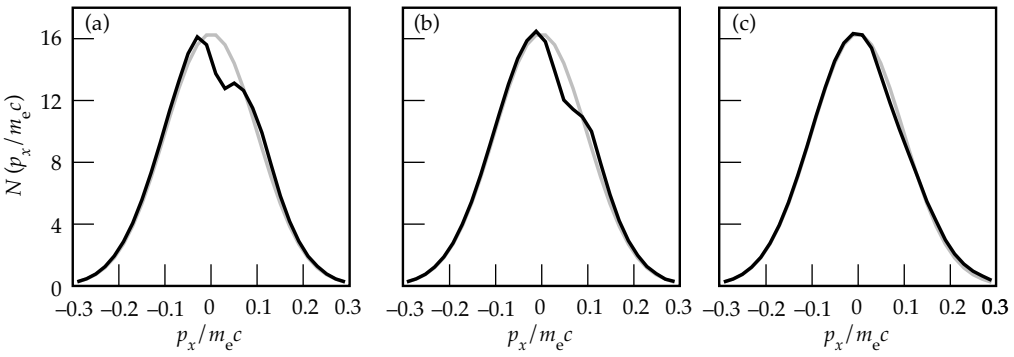

FIGURE 3. The initial (gray) and the final (black) distributions of the normalized longitudinal momentum $p_x/m_e c$, observed in three PIC simulations. The panels (a), (b), and (c) correspond to $\omega^2 c^2/\omega_p^2\ v_e^2 = 0.1$, 1.0, and 10.0, respectively.
(08-00-0296-0390pb01)

TABLE 1. Absorption coefficients η obtained from simulations with $v_e = 0.1\,c$ and various density ramp widths L. The panels (a), (b), and (c) correspond to $(\omega_p/\omega)^2$ = to 100, 50, and 20, respectively.

(a) Absorption coefficient η for $(\omega_p/\omega)^2 = 100$

$L\omega_p/c$	0.05	0.5	1	2	3	4	5	10	15	20
η (%)	9	9.5	10.5	11.5	11.5	11	10.5	7.8	5.5	4.2

(b) Absorption coefficient η for $(\omega_p/\omega)^2 = 50$

$L\omega_p/c$	0.05	0.5	1	1.5	2	2.5	3	3.5	5	7
η (%)	8	8.8	9.3	9.5	9.3	8.9	8.5	7.8	6	4.2

(c) Absorption coefficient η for $(\omega_p/\omega)^2 = 20$

$L\omega_p/c$	0.05	0.5	1	1.5	1.8	2	3
η (%)	6	6	5.5	5	4.2	4	2

For $L\omega_p/c$ sufficiently greater than unity, we expect that the absorption coefficient η will be a function of $c(\omega_p/\omega)^2/(\omega L)$. The results in Table 1 reflect such a dependence. For example, the runs of $L\omega_p/c = 20$ in panel (a), $L\omega_p/c = 7$ in panel (b), and $L\omega_p/c = 1.8$ in panel (c) all correspond to $c(\omega_p/\omega)^2/(\omega L) = 50$, and they all have η = 4.2%. The runs of $L\omega_p/c = 10$ in panel (a) and $L\omega_p/c = 3.5$ in panel (b) also have the same η of 7.8% as they both correspond to $c(\omega_p/\omega)^2/(\omega L) \approx 100$.

Summary

We modified the original sheath inverse bremsstrahlung model[14] by including the $\mathbf{v} \times \mathbf{B}$ term (velocity × magnetic field) in the Lorentz force equation. We showed that the present results are significantly different from those derived without the $\mathbf{v} \times \mathbf{B}$ term. The $\mathbf{v} \times \mathbf{B}$ term is also important in interpreting the absorption mechanism: if the $\mathbf{v} \times \mathbf{B}$ term were neglected, the absorption of the light would be incorrectly interpreted as an increase in the transverse electron temperature, which would violate the conservation of the transverse components of the canonical momentum (in the case of a normally incident laser light). We also showed that both the sheath inverse bremsstrahlung and the anomalous skin effect are limiting cases of the same collisionless absorption mechanism. We compared results from PIC plasma simulations with the absorption coefficient calculated from the linear theory and investigated the effects of finite density gradients with PIC simulations.

Acknowledgments

We are grateful for inspiring discussions with T. W. Johnston, J. P. Matte, S. C. Wilks, R. S. Walling, Z. Zinamon, and M. E. Foord.

Notes and References

1. H. M. Milchberg, R. R. Freeman, S. C. Davey, and R. M. More, *Phys. Rev. Lett.* **61**, 2364 (1988).
2. J. C. Kieffer, P. Audebert, M. Chaker, J. P. Matte, et al., *Phys. Rev. Lett.* **62**, 760 (1989).
3. R. Fedosejevs, R. Ottmann, R. Sigel, G. Kühnle, et al., *Applied Phys. B* **50**, 79 (1990).
4. R. Fedosejevs, R. Ottmann, R. Siegel, G. Kühnle, et al., *Phys. Rev. Lett.* **64**, 1253 (1990).
5. M. M. Murnane, H. C. Kapteyn, and R. W. Falcone, *Phys. Rev. Lett.* **62**, 155 (1989).
6. D. Kühlke, U. Herpes, and D. von der Linde, *Appl. Phys. Lett.* **50**, 1785 (1987).
7. C. H. Nam, W. Tighe, S. Suckewer, J. F. Seely, et al., *Phys. Rev. Lett.* **59**, 2427 (1987).
8. D. G. Stearns, O. L. Landen, E. M. Campbell, and J. H. Scofield, *Phys. Rev. A* **37**, 1684 (1988).
9. G. Kühnle, F. P. Schäfer, S. Szatmari, and G. D. Tsakiris, *Appl. Phys. B* **47**, 361 (1988).
10. J. A. Cobble, G. A. Kyrala, A. A. Hauer, A. J. Taylor, et al., *Phys. Rev. A* **39**, 454 (1989).
11. H. W. K. Tom and O. R. Wood II, *Appl. Phys. Lett.* **54**, 517 (1989).
12. S. E. Harris and J. D. Kmetec, *Phys. Rev. Lett.* **61**, 62 (1988).
13. M. Tabak, J. Hammer, M. E. Glinsky, W. L. Kruer, et al., *Phys. Plasmas* **1**, 1626 (1994).
14. P. J. Catto and R. M. More, *Phys. Fluids* **20**, 704 (1977).
15. J. P. Matte and K. Aguenaou, *Phys. Rev. A* **45**, 2588 (1992).
16. W. Rozmus and V. T. Tikhonchuk, *Phys. Rev. A* **42**, 7401 (1990).
17. E. M. Lifshitz and L. P. Pitaevskii, *Physical Kinetics* (Pergamon, Oxford, 1981).
18. S. Ichimaru, *Basic Principles of Plasma Physics* (Benjamin, Reading, MA, 1973).
19. E. S. Weibel, *Phys. Fluids* **10**, 741 (1967).
20. A. B. Langdon and B. F. Lasinski, *Methods Comput. Phys.* **16**, 327 (1976).
21. T.–Y. B. Yang, W. L. Kruer, R. M. More, and A. B. Langdon, *Phys. Plasmas* **2**, 3146 (1995).
22. R. C. Davidson, *Handbook of Plasma Physics* **1**, Eds., A. A. Galeev and R. N. Sudan (North–Holland, New York, 1983). pp. 521–585.
23. B. D. Fried and S. D. Conte, *The Plasma Dispersion Function* (Academic, New York, 1961).